ACS Catalysis

Research Article

pubs.acs.org/acscatalysis

Highly Asymmetric Phthalocyanine as a Sensitizer of Graphitic Carbon Nitride for Extremely Efficient Photocatalytic H_2 Production under Near-Infrared Light

Xiaohu Zhang,[†] Lijuan Yu,[†] Chuansheng Zhuang,[†] Tianyou Peng,*[,†] Renjie Li,*[,†] and Xingguo Li[‡]

[†]College of Chemistry and Molecular Science, Wuhan University, Wuhan 430072, People's Republic of China

[‡]Beijing National Laboratory for Molecular Sciences (BNLMS), Peking University, Beijing 100190, People's Republic of China

Supporting Information

ABSTRACT: Highly asymmetric zinc phthalocyanine derivative (Zn-*tri*-PcNc) with intense near-IR light (650−800 nm) absorption is utilized as a sensitizer to extend the spectral response region of graphitic carbon nitride (g-C_3N_4) from ∼450 nm to more than 800 nm. Ultraviolet−visible light (UV-vis) diffuse reflectance absorption spectra (DRS), photoluminescence (PL) spectra, time-resolved photoluminescence spectra (TRPS), and energy band structure analyses are adopted to investigate the photogenerated electron transfer process between Zn-*tri*-PcNc and g-C_3N_4 on both thermodynamics and dynamics aspects. After optimizing the photocatalytic condition and adding chenodeoxycholic acid (CDCA) as coadsorbent, Zn-*tri*-PcNc sensitized g-C_3N_4 photocatalyst shows a H_2 production efficiency of 125.2 μmol h^{-1} under visible/near-IR-light ($\lambda \geq 500$ nm) irradiation, corresponding to a turnover number (TON) of 5008 h^{-1} with an extremely high apparent quantum yield (AQY) of 1.85% at 700 nm monochromatic light irradiation. The present work should be the rarely fundamental investigation on the utilization of near-IR light of solar radiation for the photocatalytic H_2 production from water splitting over a dye-sensitized semiconductor.

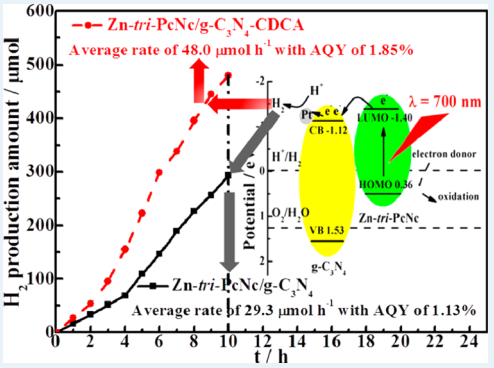

KEYWORDS: *zinc phthalocyanine derivative, photocatalysis, hydrogen production, near-IR light utilization, graphitic carbon nitride*

1. INTRODUCTION

In the past decades, more and more attention has been focused on hydrogen energy production and utilization, because of its environmental friendliness and high energy capacity. Among those approaches to H_2 production, photocatalytic H_2 production from an artificial photosynthesis system may be the most promising but challenging method, because of its potential application in the direct production of clean hydrogen energy by using water and inexhaustible solar energy.[1−6] Nevertheless, there are two major factors restricting the practical application of photocatalytic H_2 production, that is, the relatively low quantum efficiency and extremely insufficient utilization of solar light, especially the visible/near-infrared (vis/NIR) light of the solar radiation. Therefore, many approaches have been developed to extend the spectral response region of photocatalyst to visible-light region. For example, some narrow bandgap semiconductors, composite materials containing narrow and wide bandgap semiconductors, solid solutions and dye-sensitized semiconductors have been reported and used as visible-light-driven photocatalysts.[7−12] Very recently, graphitic carbon nitride (g-C_3N_4) as a novel polymer semiconductor has attracted numerous attention, because of its specific planar structure, physicochemical properties, and appropriate energy band positions for the photocatalytic water reduction and oxidation processes.[13−15] However, the bandgap of g-C_3N_4 is still as large as 2.7 eV with an absorption edge just at ∼450 nm, which largely restricts the visible-light utilization efficiency. Although many efforts such as doping with nonmetallic element and copolymerization of two or more precursor have been made to modify the physical and electron structure of g-C_3N_4, the visible-light-responsive ability and photoactivity still need further improvement urgently.[16,17]

Among the various strategies for visible-light harvesting, dye sensitization is an efficient and widely used route to extend the spectral response region of wide-band-gap semiconductors.[10−12,18] However, the mostly used Ru-complex and xanthene dyes hardly extend the spectral response region to longer than 550 nm.[6,18] Phthalocyanines (Pcs) are a type of chromophore well-known for their intrinsic absorption in the UV/blue (Soret band) and the red/near IR spectral regions (Q-band, centered at ∼650−800 nm). Moreover, the excellent photochemical/thermal stabilities and appropriate redox properties of Pcs also render them attractive as dye for the sensitization of wide-band-gap semiconductors such as TiO_2.[18] Obviously, dye sensitization of g-C_3N_4 is also an efficient way to enable the utilization of visible light of the solar radiation. Until

Received: September 29, 2013
Revised: November 9, 2013
Published: December 4, 2013

now, poly(3-hexylthiophene) (P3HT), Erythrosin B (ErB) and Eosin Y (EY) are used as sensitizers of g-C_3N_4 to enhance the photocatalytic H_2 production activity with considerable visible-light utilization efficiency and maximal responsive wavelength at ~600 nm.[19−21] However, the utilization of huge visible/near-IR light with wavelength longer than 600 nm is rarely reported, except for the MgPc-sensitized g-C_3N_4, which showed photocatalytic H_2 production activity but with rather low quantum efficiency (0.07%) at 660 nm.[22]

The recent breakthrough of phthalocyanine derivatives as a sensitizer in dye-sensitized solar cells (DSSCs) makes them also a practical dye in dye-sensitized photocatalytic system,[23] which is somewhat similar to the photovoltaic devices, in terms of the photogenerated electron transfer processes. However, the development of Pcs as sensitizers in dye-sensitized semiconductors for H_2 production still remains stagnant and never catches up with the achievement in DSSCs. Recently, zinc phthalocyanine (ZnPc) derivatives with highly asymmetric structures were successfully synthesized and used in DSSCs with considerable photovoltaic conversion efficiency.[23a] More recently, a highly asymmetric ZnPc derivative (Zn-*tri*-PcNc) was also used to sensitize TiO_2 for H_2 production, which showed a considerable photoactivity under visible-light irradiation and ca. 0.2% apparent quantum efficiency (AQY) at 700 nm monochromatic light irradiation, which is still too low to be satisfactory;[24] therefore, further investigation is urgent for the Pc-sensitized system, to more efficiently utilize the visible/near-IR light of solar energy.

Herein, by using the highly asymmetric Zn-*tri*-PcNc as a sensitizer of g-C_3N_4, it is found that the photogenerated electrons of the excited Zn-*tri*-PcNc can efficiently transfer to g-C_3N_4 based on the dynamic time-resolved photoluminescence spectra (TRPS) analyses. Since the chenodeoxycholic acid (CDCA) as a coadsorbent can hinder the Pc-dye aggregation during the dye adsorption process, which is beneficial for promoting the dye regeneration and/or the electron injection kinetics in DSSCs,[23,25] the effect of CDCA as coadsorbent on the photocatalytic H_2 production efficiency of Zn-*tri*-PcNc/g-C_3N_4 are also investigated. It is found that CDCA coadsorption with Zn-*tri*-PcNc can also improve the electron injection efficiency and retard the charge recombination, and thus resulting in significantly improved photoactivity for H_2 production. Especially, Zn-*tri*-PcNc/g-C_3N_4 with CDCA as coadsorbent exhibits a H_2 production efficiency of 125.2 μmol h^{-1} with a turnover number (TON) of ~5008 h^{-1} under visible-light ($\lambda \geq 500$ nm) irradiation; moreover, it gives an extremely high apparent quantum yield (AQY) of 1.85% at 700 nm monochromatic light irradiation, improved by a factor of ~9.3, compared with the previously reported one (0.2%) of a similar dye-sensitized TiO_2 system.[24] The above results show the promising application of phthalocyanines in photocatalytic H_2 production system for more efficiently utilizing the solar radiation with wavelength longer than 600 nm or even 700 nm, which has never been reached by those mostly used Ru-complex and xanthene dyes, as previously mentioned.[18]

2. EXPERIMENTAL SECTION

Material Preparation and Characterization. Graphitic carbon nitrides (g-C_3N_4) were synthesized according to our previous reports.[26] Typically, the precursor (urea) was kept in a crucible with a cover and heated at 580 °C for 3 h with a heating rate of 5 °C min^{-1}. The yellow-colored product was washed by nitric acid (0.1 M) and distilled water, and then dried at 70 °C overnight to obtain the product (g-C_3N_4). Co-catalyst platinum was loaded on g-C_3N_4 through a photodeposition procedure. Typically, g-C_3N_4 (0.2 g) was added to 40 mL water and 10 mL methanol, the suspension was dispersed in an ultrasonic bath for 10 min, and then irradiated by a 500-W high-pressure mercury lamp for 3 h under stirring after adding 0.134 mL of H_2PtCl_6 solution (0.077 M). The product was separated by centrifugation and washed with water, and then dried at 70 °C overnight to obtain 1.0 wt % Pt-load g-C_3N_4 (Pt/g-C_3N_4).

Zinc phthalocyanine derivative (Zn-*tri*-PcNc) was synthesized according to our previous report,[23a] which is highly asymmetric tribenzonaphtho-condensed tetraazaporphyrine (PcNc) designed on the concept of "pull−push" effect with one carboxyl group at one naphtha-part peripheral position and electron-releasing group (*t*-Bu) at the other three benzo-condensed positions. The basic structures of Zn-*tri*-PcNc and g-C_3N_4 are shown in Figure 1. XRD patterns of g-C_3N_4

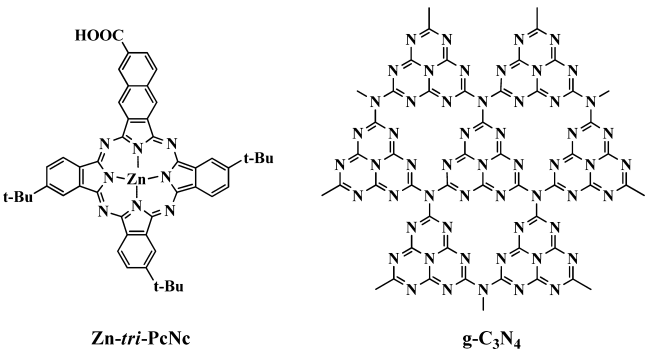

Figure 1. Structures of zinc phthalocyanine derivative (Zn-*tri*-PcNc) and an idealized g-C_3N_4.

and Zn-*tri*-PcNc/g-C_3N_4 (see Figure S1a in the Supporting Information) indicate that the bare g-C_3N_4 exhibits a typical diffraction pattern consistent with the literature,[13,26] and XRD pattern of Zn-*tri*-PcNc/g-C_3N_4 is very similar to that of g-C_3N_4, implying the low amount and high dispersity of Zn-*tri*-PcNc on g-C_3N_4 surfaces.

Dye-sensitized Pt/g-C_3N_4 (Zn-*tri*-PcNc/g-C_3N_4) was prepared by an impregnation method. Typically, 0.1 g Pt/g-C_3N_4 was mixed with 3 mL of Zn-*tri*-PcNc ethanol solution containing different CDCA concentrations under stirring for 12 h and then the product was filtrated through a 0.45-μm nylon filter and dried at room temperature overnight. The adsorbed amount of Zn-*tri*-PcNc was calculated according to the absorbance difference between the initial Zn-*tri*-PcNc solution and the filtered solution after the sensitization process. The dye desorption was carried out by dispersing the dye-sensitized photocatalyst before or after irradiation in 0.1 M NaOH ethanol/water (v/v = 1:1) solution under ultrasonication, and then separated by centrifugation, and the liquid supernatant was detected by a UV-vis-NIR spectrophotometer.

The crystal phases analyses were carried out on a Bruker D8-Avance X-ray diffractometer (XRD) with Cu Kα radiation (λ = 0.154178 nm) at 40 kV and 40 mA. UV-vis diffuse reflectance absorption spectroscopy (DRS) spectra were obtained with a Shimadzu UV-3600 UV−vis-NIR spectrophotometer that was equipped with an integrating sphere. Photoluminescence (PL) spectra were determined by using a Hitachi Model F-4500 fluorescence spectrophotometer. Time-resolved photoluminescence spectroscopy (TRPS) spectra were obtained on a Model FES 920 system (Edinburgh Instruments) with an excitation wavelength of 377 nm and detection wavelength of 711 nm. The films for PL and TRPS measurements were prepared by the following methods: 0.2 g Zn-*tri*-PcNc/g-C_3N_4 or Zn-*tri*-PcNc/Al_2O_3 was mixed with 0.2 mL of water under ultrasonic treatment for 30 min, and then the corresponding film was prepared on a quartz plate, using a doctor-blade technique, followed by drying under vacuum.

Photocatalytic Property Tests. The photocatalytic H_2 production reaction was carried out in a typical photocatalytic system.[6,24] Typically, the photoreaction system contains 10 mg of Zn-*tri*-PcNc/g-C_3N_4 as a photocatalyst, 10 mL of water, and 88 mg of ascorbic acid

dx.doi.org/10.1021/cs400863c | ACS Catal. 2014, 4, 162−170

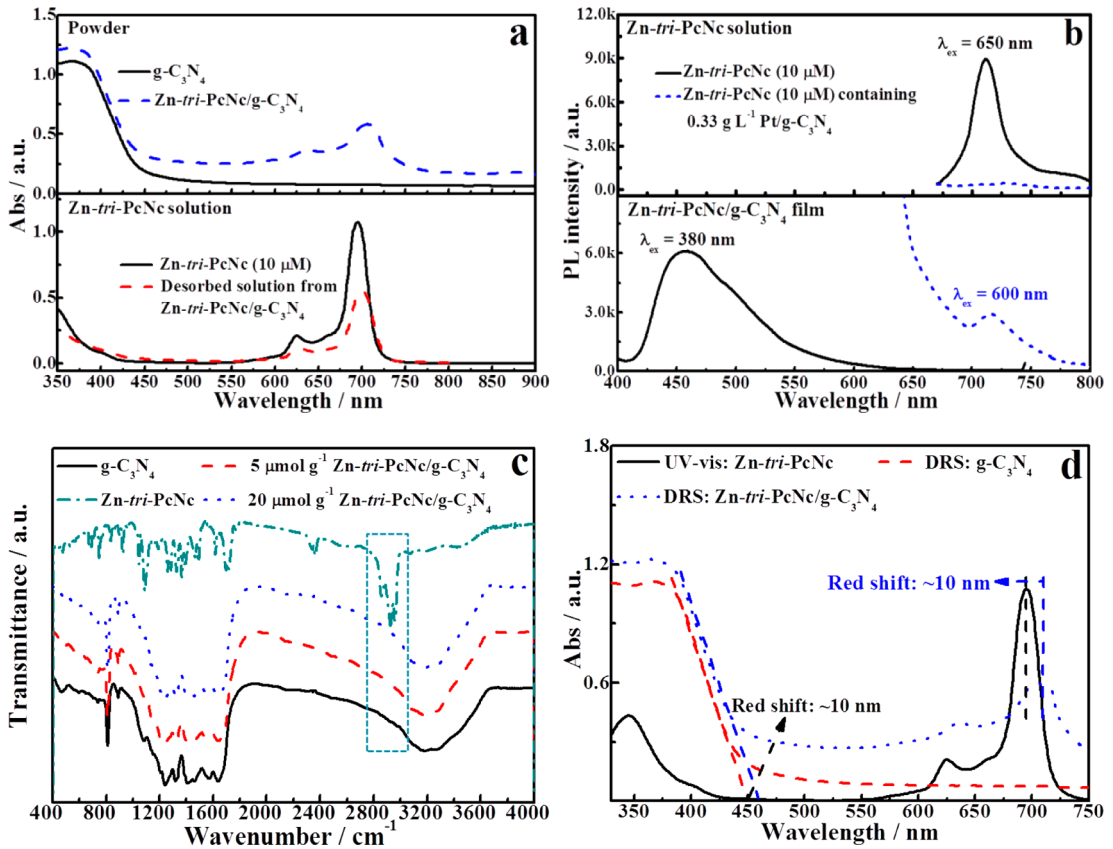

Figure 2. (a) Diffuse reflectance absorption spectroscopy (DRS) spectra of g-C_3N_4 and Zn-*tri*-PcNc/g-C_3N_4 (above) and UV-vis spectra of 10 μM Zn-*tri*-PcNc solution and the desorbed solution of Zn-*tri*-PcNc/g-C_3N_4 (below); (b) photoluminescence (PL) spectra of 10 μM Zn-*tri*-PcNc solution with/without adding Pt/g-C_3N_4 (above, slit width: EX 5 nm, EM 10 nm) and Zn-*tri*-PcNc/g-C_3N_4 film under 380 or 600 nm light excitation (below, slit width: EX 5 nm, EM 5 nm); (c) Fourier transform infrared (FTIR) spectra of g-C_3N_4 and Zn-*tri*-PcNc/g-C_3N_4; and (d) absorption spectra comparison of Zn-*tri*-PcNc before and after adsorbing g-C_3N_4.

(AA, 50 mM) as an electron donor. Long-wavelength pass filter ($\lambda \geq$ 420, 500 nm) or band-pass filter ($\lambda = 700 \pm 10$ nm, etc.) was equipped with a 300-W xenon lamp to get corresponding light irradiation. The turnover number (TON) and apparent quantum yield (AQY) were measured and calculated according to the following equations:[6,24]

$$\text{TON} = \frac{2 \times \text{number of evolved } H_2 \text{ molecules}}{\text{number of dye molecules adsorbed}} \quad (1)$$

$$\text{AQY}\,(\%) = \frac{2 \times \text{number of evolved } H_2 \text{ molecules}}{\text{number of incident photons}} \times 100 \quad (2)$$

Photoelectrochemical Measurements. A CHI Model 618C electrochemical analyzer with a standard three-electrode system was used to record transient photocurrent behavior of the dye-sensitized g-C_3N_4, where a platinum wire, a platinum plate, and Ag/AgCl work act as the work, counter, and reference electrode, respectively. In addition, the three electrodes were immersed into a suspension containing 10 mg of g-C_3N_4 (or Zn-*tri*-PcNc/g-C_3N_4), 1.0 M NaOH solution, and 5 mg of methyl viologen (MV) as electron media, which was continuously purged by N_2 flow to remove O_2 before light irradiation.[26,27]

3. RESULTS AND DISCUSSION

Spectral Property Analyses of Zn-*tri*-PcNc/g-C_3N_4. UV-vis diffuse reflectance absorption spectroscopy (DRS) spectra of g-C_3N_4 and Zn-*tri*-PcNc/g-C_3N_4 are shown in Figure 2a. For comparison, UV-vis absorption spectrum of Zn-*tri*-PcNc solution is also listed in Figure 2a. As can be seen, Zn-*tri*-PcNc solution shows an excellent visible/near-IR responsive property with an intense absorption band at ~700 nm (Q-band, ε = 106 000 L mol^{-1} cm^{-1}), which is favorable and significant for the visible/near-IR-light induced photocatalytic H_2 production. Generally, the dye adsorption on semiconductor is a prerequisite factor for the photogenerated electron transfer and H_2 production in a dye-sensitized system.[28] As can be seen from Figure 2a, Zn-*tri*-PcNc/g-C_3N_4 exhibits much broader absorption band through the entire visible/near-IR light region from 400 nm to 850 nm, compared to the pristine g-C_3N_4, which only shows an absorption onset at ~450 nm. Moreover, the spectral absorption property of Zn-*tri*-PcNc/g-C_3N_4 can be markedly enhanced along with increasing the adsorbed amount of Zn-*tri*-PcNc (see Figure S1b in the Supporting Information). To further clarify whether dye molecules changed or not after the adsorption process, the dye was desorbed from Zn-*tri*-PcNc/g-C_3N_4, and the corresponding desorbed Zn-*tri*-PcNc solution shows a UV-vis absorption spectrum (Figure 2a) very similar to the original solution on the aspect of curve shape and peak position. This qualitatively indicates that Zn-*tri*-PcNc can remain unchanged before and after the adsorption process.

Photoluminescence (PL) is an effective and commonly used method to investigate the electron transfer property of the semiconductor.[21,29,30] Therefore, the effect of g-C_3N_4 on the PL intensity of Zn-*tri*-PcNc solution was investigated and shown in Figure 2b. Zn-*tri*-PcNc solution shows an intense emission peak centered at ~711 nm with excitation wavelength of 650 nm, which should be caused by the photogenerated electron−hole pair recombination of the dye.[21,24] However, the

dx.doi.org/10.1021/cs400863c | ACS Catal. 2014, 4, 162−170

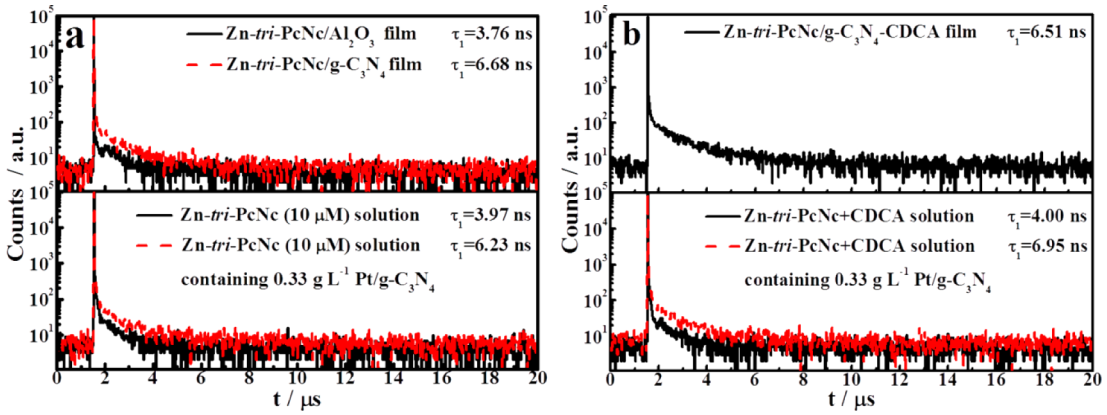

Figure 3. (a) Time-resolved fluorescence decay curves of Zn-*tri*-PcNc/Al_2O_3 and Zn-*tri*-PcNc/g-C_3N_4 films (above), and Zn-*tri*-PcNc solution (10 μM) with/without adding g-C_3N_4 (below); (b) effects of CDCA on the time-resolved fluorescence decay of Zn-*tri*-PcNc/g-C_3N_4 film (above) or Zn-*tri*-PcNc solution with/without adding g-C_3N_4 (below). Excitation and detection wavelengths are 377 and 711 nm, respectively.

PL intensity of Zn-*tri*-PcNc solution can be markedly quenched by adding Pt/g-C_3N_4. Since the absorption spectrum of g-C_3N_4 shows no overlap with the emission spectrum of Zn-*tri*-PcNc (see Figure 2a and 2b), this PL quenching of Zn-*tri*-PcNc solution by Pt/g-C_3N_4 should be ascribed to the efficient electron transfer process.[21,30] That is, the photogenerated electrons of the excited Zn-*tri*-PcNc can be transferred to the conduction band (CB) of g-C_3N_4. This conjecture is reasonable by considering the relative energy band levels of Zn-*tri*-PcNc and g-C_3N_4 because the lowest unoccupied molecular orbital (LUMO) level of Zn-*tri*-PcNc is −1.40 eV,[23a] which is sufficiently negative than the CB level (−1.12 eV) of g-C_3N_4,[13,22] indicating that the electron transfer from the excited Zn-*tri*-PcNc to g-C_3N_4 is favorable thermodynamically.

To further investigate the interaction between Zn-*tri*-PcNc and g-C_3N_4, the PL spectra of Zn-*tri*-PcNc/g-C_3N_4 film fabricated on quartz plate under different excitation wavelength were measured and shown in Figure 2b. As can be seen, an intense emission band at ∼455 nm under excitation wavelength of 380 nm and a weak emission band at ∼715 nm under excitation wavelength of 600 nm can be observed, which should be attributed to the charge recombination processes of g-C_3N_4 and Zn-*tri*-PcNc, respectively. The emission peak ascribable to the electron transfer between g-C_3N_4 and Zn-*tri*-PcNc is not detected unfortunately, which may be ascribed to the unusual weak emission intensity and the limited detection range of the present fluorescence spectrophotometer. Nevertheless, the much weaker emission peak (at ∼715 nm) of Zn-*tri*-PcNc/g-C_3N_4 film, compared to the Zn-*tri*-PcNc solution, still implies the quenching effect of Pt/g-C_3N_4 on the excited Zn-*tri*-PcNc. As can be seen from the FTIR spectra in Figure 2c, the pristine g-C_3N_4 exhibits characteristic IR absorption peaks similar to that in the previous literature.[29] The absorption band at 1636 cm^{-1} can be ascribed to the C−N stretching vibration, while the four strong peaks at 1247, 1329, 1423, and 1569 cm^{-1} to the CN heterocycle stretching of g-C_3N_4, and a shoulder broad band near 3166 cm^{-1} corresponds to the stretching mode of terminal −NH groups at the defect sites of the aromatic ring.[29] Zn-*tri*-PcNc shows the characteristic phthalocyanine dianion IR bands at ∼1090 cm^{-1} attributed to the symmetric bending of C−H in the $-CH_3$ groups in side chains of Pc rings, together with the isoindole stretching vibrations.[23a] Moreover, an intensive absorption bands at 3009−2750 cm^{-1} attributable to stretching vibrations of −COOH in the asymmetric ZnPc derivative can also be observed.[23a] However, the intensive absorption bands of −COOH cannot be observed from the FTIR spectra of the Zn-*tri*-PcNc/g-C_3N_4 (either with 5 or even 20 μmol g^{-1} dye-adsorbed amount), which show almost the same IR absorption peak positions as that of the pristine g-C_3N_4, indicating that there is limited chemical interaction existing between Zn-*tri*-PcNc and g-C_3N_4, which may be difficult to be detected using the FTIR spectrum. Since there are −COOH groups in Zn-*tri*-PcNc and terminal −NH groups in g-C_3N_4 as mentioned above, it is possible that the formation of a chemical interaction between Zn-*tri*-PcNc and g-C_3N_4 via a condensation reaction between the terminal −NH groups in g-C_3N_4 and the −COOH groups in Zn-*tri*-PcNc during the present chemical adsorption process. Furthermore, $\pi-\pi$ staking interaction between Zn-*tri*-PcNc and g-C_3N_4 may also exist in terms of their similar planar and π-conjugated structures. This conjecture may be validiated by the changes in the photophysical property of Zn-*tri*-PcNc and g-C_3N_4 shown in Figure 2d. As can be seen, both of the optical absorption band and onset of Zn-*tri*-PcNc/g-C_3N_4 are red-shifted ∼10 nm, compared to the pristine g-C_3N_4 (at ∼450 nm) and Zn-*tri*-PcNc (at ∼700 nm) solution, respectively. It may be caused by the $\pi-\pi$ staking interaction between the large conjugated structures of g-C_3N_4 and Zn-*tri*-PcNc. Based on the above observations and discussion, it can be concluded that Zn-*tri*-PcNc/g-C_3N_4 with close interfacial connections was achieved, and this connection may serve as electron migration paths to promote the charge separation, and induce a synergetic effect for improved photoactivity.

The dynamic electron transfer process between Zn-*tri*-PcNc and g-C_3N_4 can be further investigated by using time-resolved photoluminescence spectra (TRPS) shown in Figure 3, which contains useful information of the electron recombination/transfer processes between Zn-*tri*-PcNc and g-C_3N_4. The fluorescence lifetimes of Zn-*tri*-PcNc solution with or without adding Pt/g-C_3N_4 and Zn-*tri*-PcNc/g-C_3N_4 films were obtained by fitting the time-resolved fluorescence decay curves with the following exponential fitting equation:

$$\text{Fit} = A + B_1 \exp\left(-\frac{t}{\tau_1}\right) + B_1 \exp\left(-\frac{t}{\tau_2}\right) + B_1 \exp\left(-\frac{t}{\tau_3}\right) \quad (3)$$

dx.doi.org/10.1021/cs400863c | ACS Catal. 2014, 4, 162−170

Table 1. Time-Resolved Fluorescence Decay Data of Zn-*tri*-PcNc Solution with/without Adding Pt/g-C_3N_4 and Zn-*tri*-PcNc/g-C_3N_4 Films Derived from Figure 3[a]

system	τ_1 [ns] (Rel%)	τ_2 [ns] (Rel%)	τ_3 [ns] (Rel%)	τ [ns]	χ^2
(s) Zn-*tri*-PcNc	3.97 (98.9%)	50.43 (0.6%)	770.93 (0.5%)	3.97	1.225
(s) Zn-*tri*-PcNc+g-C_3N_4	6.23 (92.8%)	62.28 (3.3%)	1165.95 (4.0%)	6.23	1.324
(f) Zn-*tri*-PcNc/Al_2O_3	3.76 (99.0%)	695.77 (0.7%)	4272.3 (0.3%)	3.76	1.303
(f) Zn-*tri*-PcNc/g-C_3N_4	6.68 (83.8%)	83.38 (5.1%)	1447.3 (11.6%)	6.68	1.295
(s) Zn-*tri*-PcNc+CDCA	4.00 (99.5%)	50.47 (0.3%)	762.89 (0.2%)	4.00	1.156
(s) Zn-*tri*-PcNc+g-C_3N_4+CDCA	6.95 (84.9%)	57.76 (7.0%)	1287.7 (8.1%)	6.95	1.346
(f) Zn-*tri*-PcNc/g-C_3N_4−CDCA	6.51 (81.4%)	99.98 (4.5%)	1466.2 (14.1%)	6.51	1.273

[a]Notes: (s) and (f) represent solution and film, respectively. CDCA/Zn-*tri*-PcNc mole ratio = 50, 10 μM Zn-*tri*-PcNc solution, 5 μmol g^{-1} Zn-*tri*-PcNc/g-C_3N_4 film; τ_1, τ_2, and τ_3 are fluorescence lifetimes, and τ is the final fluorescence lifetime of the corresponding system according to τ_1, which dominates the lifetimes with almost 100% relative fraction (Rel%); Excitation and detection wavelength is 377 and 711 nm, respectively.

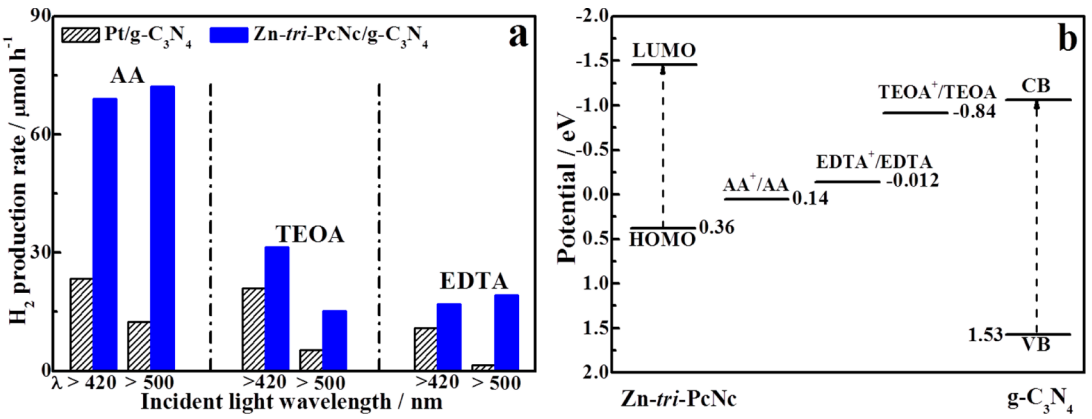

Figure 4. (a) Photocatalytic H_2 production rates over Zn-*tri*-PcNc/g-C_3N_4 in the presence of various electron donors under different light irradiation conditions. Conditions: 10 mg 1.0 wt % Pt-loaded catalyst with 5.0 μmol g^{-1} Zn-*tri*-PcNc, 10 mL of water containing 50 mM AA, 10 vol % TEOA or 10 mM EDTA; (b) the relative positions of the sacrificial reagents' redox potentials and the CB/VB (for g-C_3N_4), as well as the HOMO/LUMO (for Zn-*tri*-PcNc) levels.

where A, B_1, B_2, and B_3 are constants and obtained after fitting every decay curve.

The corresponding fitted fluorescence decay data are listed in Table 1. As can be seen from Figure 3a and Table 1, the fluorescence lifetime (τ_1) is 3.97 ns for Zn-*tri*-PcNc solution, and it is obviously prolonged to 6.23 ns after adding Pt/g-C_3N_4. That is, 3.97 ns is the intrinsic fluorescence lifetime of Zn-*tri*-PcNc solution, which is related with its photogenerated charge recombination rate under light excitation. The prolonged fluorescence lifetime after adding Pt/g-C_3N_4 indicates that the charge recombination rate of Zn-*tri*-PcNc is restrained by g-C_3N_4 through the electron transfer from the excited Zn-*tri*-PcNc to g-C_3N_4. Moreover, the fluorescence lifetime of Zn-*tri*-PcNc/Al_2O_3 film is very similar to the value of Zn-*tri*-PcNc solution, indicating the photogenerated electrons of the excited Zn-*tri*-PcNc cannot transfer to Al_2O_3 due to its insulating property; while the fluorescence lifetime of Zn-*tri*-PcNc/g-C_3N_4 film is obvious longer than Zn-*tri*-PcNc solution. This result on fluorescence lifetime of the films is similar to the corresponding solution, and confirms the retarding effect of the excited Zn-*tri*-PcNc's charge recombination. These spectral properties indicate that the Zn-*tri*-PcNc/g-C_3N_4 can be activated by visible/near-IR light, and the photogenerated electrons of the excited Zn-*tri*-PcNc can be efficiently injected into g-C_3N_4 film and further trapped by the loaded Pt particles to react with H^+ from water for H_2 production.

Photocatalytic Activity Analyses of Zn-*tri*-PcNc/g-C_3N_4. The photocatalytic H_2 production reaction of a dye-sensitized semiconductor system is usually affected by series of conditions such as electron donors, co-catalyst Pt, irradiation wavelength and time, dye-adsorbed amount and so on.[18] Herein, three commonly used sacrificial reagents—triethanolamine (TEOA), ethylenediamine tetraacetic acid disodium salt (EDTA), and ascorbic acid (AA)—were adopted to investigate the H_2 production rate over Zn-*tri*-PcNc/g-C_3N_4 under different light irradiation conditions, and the corresponding results are shown in Figure 4a. As can be seen, obvious H_2 production can be obtained over Zn-*tri*-PcNc/g-C_3N_4 in the presence of the above-mentioned sacrificial reagents under both $\lambda \geq 420$ nm and $\lambda \geq 500$ nm light irradiation, which is much higher than that of the pristine g-C_3N_4 under the same photoreaction conditions. This result indicates the photosensitization of the present Pcs dye on the g-C_3N_4.

Among those sacrificial reagents tested, EDTA as electron donors shows the lowest photoactivity for H_2 production, while the best photoactivity can be obtained over Zn-*tri*-PcNc/g-C_3N_4 by using AA as sacrificial reagent as can be observed from Figure 4a. Gererally, the sacrificial reagent significantly affects the photoactivity of a dye-sensitized semiconductor system.[31−33] For example, it has been reported that sacrificial reagents, such as EDTA, TEOA and diethanolamine (DEOA), show markedly different photoactivities for H_2 production in an Eosin Y-sensitized CuO/TiO_2 system.[31] Choi and co-workers also reported that an organic dye-sensitized TiO_2 could work for photocatalytic H_2 production in the presence of TEOA and EDTA as electron donor but with obviously different photoactivities.[32] According to the previous reports,[23a,31−34] the relative positions of the redox potentials of the three

dx.doi.org/10.1021/cs400863c | ACS Catal. 2014, 4, 162−170

sacrificial reagents used and the CB/VB (for g-C_3N_4) as well as the HOMO/LUMO (for Zn-*tri*-PcNc) levels are shown in Figure 4b. As can be seen, the LUMO level of Zn-*tri*-PcNc is more negative than g-C_3N_4 CB, while its HOMO level is more positive than the redox potentials of TEOA, EDTA, and AA; therefore, the overall charge transfers are allowed and, consequently, the H_2 production is possible.[32] By comparing the redox potentials of sacrificial reagents and the HOMO level of Zn-*tri*-PcNc, it can be concluded that the regeneration of oxidized dye is more favored in TEOA and EDTA than in AA, and the HOMO level of Zn-*tri*-PcNc is very close to the one-electron redox potential of AA (compared to that of EDTA and TEOA), which should retard the regeneration of the oxidized dye by AA and, consequently, increases the recombination between the oxidized dye and ejected electrons. Conversely, AA as sacrificial reagent shows much better photoactivity than TEOA or EDTA, as previously mentioned. This strongly suggests that dye-sensitized H_2 production system is sensitive not only to the energy levels but also to the electron transfer kinetics that are related to molecular interaction among dyes, g-C_3N_4 surface, and electron donors.[31,32] It should be noted that the adsorption and desorption of dyes is highly sensitive to pH value due to different acid-dissociation behaviors between dyes and semiconductor.[31−33] In this regard, the probable reason might be the differences in the acidity or basicity of the sacrificial reagent solutions, which may further influence the approach to the oxidized dye molecules, since it has reported that pH-dependent H_2 production can be obtained using EDTA or TEOA as a sacrificial reagent in a semiconductor system.[32] Possibly, the use of acidic AA as an electron donor is easier to contact with the oxidized dye than the basic TEOA, resulting in more-efficient dye regeneration rates and then the better photoactivity. Moreover, EDTA is a more strongly competitive electron donor than TEOA on a dye-sensitized semiconductor, since EDTA has been known to hamper the adsorption of dye-containing carboxylic acid as the anchoring group; when dyes and EDTA are simultaneously adsorbed onto TiO_2,[35] it is possible for the present preadsorbed dye to be desorbed from semiconductor during (or by) photolysis in the presence of EDTA,[32] which would further influence the dye's adsorption/desorption processes in the aqueous sensitized semiconductor suspension, then resulting in the lowest photoactivity (as compared to the AA or TEOA as an electron donor) as shown in Figure 4a. Of course, the above suppositions need further experimental facts to confirm, which is under progress.

As can be seen from Figure 4a, Zn-*tri*-PcNc/g-C_3N_4 shows much better photoactivity for H_2 production than the pristine g-C_3N_4 in the presence of AA under $\lambda \geq 420$ (or 500) nm light irradiation. Moreover, Zn-*tri*-PcNc/g-C_3N_4 under $\lambda \geq 500$ nm light irradiation has a slightly higher photoactivity than that under $\lambda \geq 420$ nm light irradiation in the presence of AA, while the pristine g-C_3N_4 under $\lambda \geq 500$ nm light irradiation shows relatively lower photoactivity than that under $\lambda \geq 420$ nm light irradiation. This reversed photoactivity can be ascribed to the differences existing in the light absorption properties between the Zn-*tri*-PcNc and g-C_3N_4 and in the transmissivity between the $\lambda \geq 500$ nm and $\lambda \geq 420$ nm cutoff filters. As can be seen from Figure S2 in the Supporting Information, the light transmissivity (~92%) and intensity (334.8 mW cm^{-2}) of $\lambda \geq 500$ nm cutoff filter are larger than that (~85% transmissivity and 328.4 mW cm^{-2} intensity) of $\lambda \geq 420$ nm cutoff filter. On the one hand, the above better photoactivity of Zn-*tri*-PcNc/g-C_3N_4 under $\lambda \geq 500$ nm light irradiation can be mainly attributed the higher transmitting light intensity of the $\lambda \geq 500$ nm cutoff filter than that of the $\lambda \geq 420$ nm cutoff filter, because the light absorption in the range of 420−500 nm of Zn-*tri*-PcNc, which acts as a sensitizer to harvest light in the Zn-*tri*-PcNc/g-C_3N_4 system, is very limited, as can be seen from Figure 2a. On the other hand, the relatively lower photoactivity of the pristine g-C_3N_4 under $\lambda \geq 500$ nm light irradiation (than that under $\lambda \geq 420$ nm light irradiation) can be ascribed to the removal of the light absorption in the range of 420−450 nm (the absorption onset) of g-C_3N_4 by the $\lambda \geq 500$ nm cutoff filter, as can be seen from Figure 2aa as well as Figure S2 in the Supporting Information, and the higher light transmissivity and intensity of $\lambda \geq 500$ nm cutoff filter would not contribute H_2 production because the absorption onset of g-C_3N_4 is just at ~450 nm. Anyway, it can be concluded that the better photoactivity of Zn-*tri*-PcNc/g-C_3N_4 under $\lambda \geq 500$ nm light irradiation can be ascribed to the relatively higher transmitting light intensity of the $\lambda \geq 500$ nm cutoff filter. Therefore, AA as sacrificial reagent and $\lambda \geq 500$ nm light irradiation are used to further optimize the photoreaction condition of Zn-*tri*-PcNc/g-C_3N_4, and the corresponding results are shown in Figure S3 in the Supporting Information. As can be seen, optimal photoreaction conditions would be: 10 mg 0.5 wt % Pt-loaded g-C_3N_4 sensitized with dye, dispersed in 10 mL of water containing 50 mM AA without adjusting the pH value.

In addition to the above conditions, as major influencing factors, the dye adsorbed amount and coadsorbent CDCA amount in dye-sensitized photocatalytic system should also be noted. Figure 5 shows the effects of Zn-*tri*-PcNc adsorbed amount on the photoactivity for H_2 production over Zn-*tri*-PcNc/g-C_3N_4. As light harvester and photoelectron generator, Zn-*tri*-PcNc plays the most major role in a dye-sensitized photocatalytic system. As can be seen, the photocatalytic H_2 production rate is improved dramatically by enhancing the adsorbed amount of Zn-*tri*-PcNc. However, the photoactivity remained stable when the adsorbed amount of Zn-*tri*-PcNc exceeded 5.0 μmol g^{-1}. This phenomenon should be reasonable in terms of the competitive relation between light harvesting and active sites for H_2 production. On the other hand, CDCA as a coadsorbent is commonly used in ZnPc-sensitized solar cells to improve cell performance due to the reduced dye

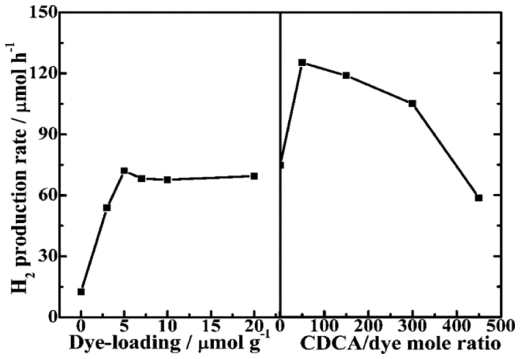

Figure 5. Effects of Zn-*tri*-PcNc and CDCA amount on the photoactivity for H_2 production over Zn-*tri*-PcNc/g-C_3N_4. If otherwise stated, the conditions are as follows: 10 mg of 1.0 wt % Pt-loaded catalyst with 5.0 μmol g^{-1} Zn-*tri*-PcNc, 10 mL of water containing 50 mM AA with the pH value unadjusted (1.5−1.8), and $\lambda \geq 500$ nm light irradiation.

dx.doi.org/10.1021/cs400863c | ACS Catal. 2014, 4, 162−170

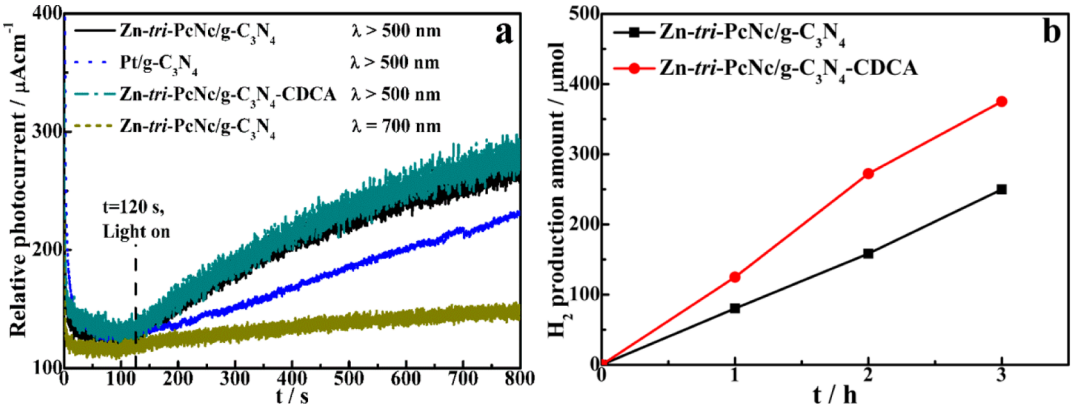

Figure 6. Effects of coabsorbent CDCA on (a) the transient photocurrent behaviors and (b) the photoactivity of Zn-*tri*-PcNc/g-C_3N_4 under optimal photoreaction conditions and $\lambda \geq 500$ nm light irradiation.

aggregation.[23,25] However, CDCA has never been adopted in a dye-sensitized photocatalytic system, as far as we know. Therefore, we attempt to introduce CDCA into Zn-*tri*-PcNc/g-C_3N_4 during the photocatalyst preparation procedure and investigate its effect on the photoactivity; the corresponding results are also shown in Figure 5. As can be seen, photocatalytic H_2 production rate was markedly improved by adding CDCA. Especially, when CDCA/Zn-*tri*-PcNc mole ratio is 50, Zn-*tri*-PcNc/g-C_3N_4 shows the best photocatalytic H_2 production activity (125.2 μmol h^{-1}) with a TON of 5008 h^{-1} under $\lambda \geq 500$ nm light irradiation, improved by 50.5%, compared with the photoreaction system without CDCA.

The role of CDCA in the Zn-*tri*-PcNc/g-C_3N_4 system can be further investigated using TRPS spectra (Figure 3b) and DRS spectra (Figure S4 in the Supporting Information). As can be seen from Figure 3b and Table 1, the fluorescence lifetimes (τ_1) of Zn-*tri*-PcNc did not change obviously after the coadsorption of CDCA either in solutions or in films. Namely, CDCA hardly affects or hinders the photogenerated electrons of the excited Zn-*tri*-PcNc transferring to g-C_3N_4. On the other hand, addition of CDCA can influence the absorbance ratio ($Abs_{705\ nm}/Abs_{636\ nm}$) at ~705 nm (monomer peak) and ~636 nm (aggregation peak), although the spectral response region and position of the photocatalyst are unchanged, as shown in Figure S4 in the Supporting Information. The absorbance ratio is increased from 1.59 to 1.79 when the CDCA/Zn-*tri*-PcNc molar ratio is enhanced from 0 to 50, indicating that the degree of aggregation of Zn-*tri*-PcNc can be reduced by the introduction of CDCA. However, excessive CDCA will influence the active sites for H_2 production, which is harmful to the photoactivity of Zn-*tri*-PcNc/g-C_3N_4; therefore, an optimal CDCA/Zn-*tri*-PcNc molar ratio is selected to be 50 in the present photocatalytic system.

Except for the restraining aggregation effect of CDCA, more-efficient photogenerated electron injection efficiency is another reason for the improvement of photoactivity when CDCA is added. It can be validated by the transient photocurrent spectra shown in Figure 6a. As can be seen, the Zn-*tri*-PcNc/g-C_3N_4 with CDCA coadsorption exhibits higher photocurrent response under $\lambda \geq 500$ nm light irradiation, indicating more fast and efficient photogenerated electron injection from the excited Zn-*tri*-PcNc to g-C_3N_4. Figure 6b exhibits photocatalytic H_2 production rate over Zn-*tri*-PcNc/g-C_3N_4 with or without CDCA coadsorption. As can be seen, Zn-*tri*-PcNc/g-C_3N_4 with CDCA coadsorption exhibits an average photoactivity (125.2 μmol h^{-1}) with TON = 5008 h^{-1} during $\lambda \geq 500$ nm light irradiation for 3 h, which is much higher than that (83.2 μmol h^{-1}) of the same system but without CDCA. It also indicating CDCA as coadsorbent can promote the photogenerated electron injection/transfer efficiency in the present Zn-*tri*-PcNc/g-C_3N_4 system.

The photocatalytic H_2 production amount over photocatalyst is also measured under various monochromatic light irradiation with λ= 420, 435, 450, 500, 520, 550, 570, 600, 635, 660, 685, 700,735, 760, 785, and 800 ± 10 nm, using corresponding narrow band-pass filters, and then the wavelength-dependent AQY values are calculated based on the H_2 production rate and corresponding incident monochromatic light intensity according to eq 2. Figure 7 shows the comparison of the DRS spectra

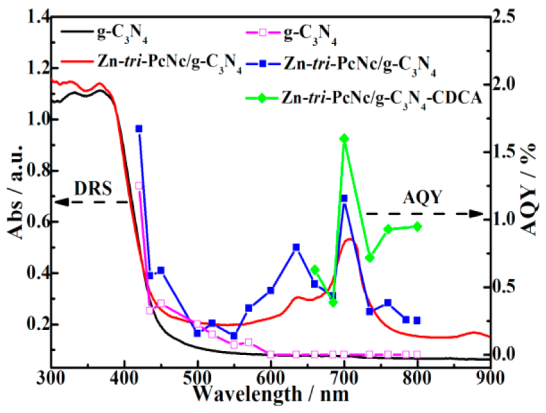

Figure 7. Comparison of DRS spectra and AQY values of g-C_3N_4 and Zn-*tri*-PcNc/g-C_3N_4 under optimal photoreaction conditions and different monochromatic light irradiation.

and AQY values as a function of the incident monochromatic light wavelength of g-C_3N_4 and Zn-*tri*-PcNc/g-C_3N_4 with/without coadsorption of CDCA. As can be seen, all samples exhibit AQY values as the same changing tendency as their respective DRS spectrum. It is worthy of mention that Zn-*tri*-PcNc/g-C_3N_4 shows impressive AQY values in all visible/near-IR light region, especially in the region of 550−800 nm, while Pt/g-C_3N_4 only shows very low AQY values when the wavelength of light radiation is longer than 500 nm. This result indicates that the photoactivity for H_2 production over Zn-*tri*-PcNc/g-C_3N_4 is indeed governed by the Zn-*tri*-PcNc adsorbed on g-C_3N_4. Based on the above results and discussion,

dx.doi.org/10.1021/cs400863c | ACS Catal. 2014, 4, 162−170

the proposed photocatalytic H_2 production mechanism over Zn-*tri*-PcNc/g-C_3N_4 is shown in Figure 8. Briefly speaking, the

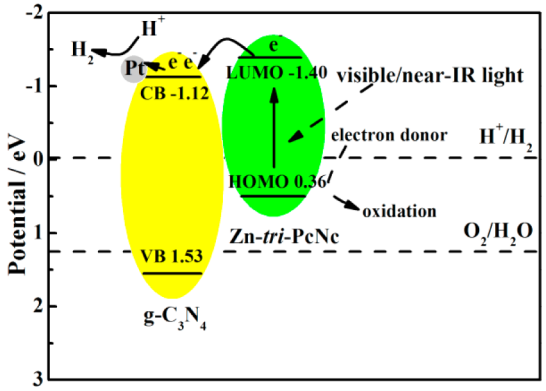

Figure 8. Proposed photocatalytic H_2 production mechanism of the Zn-*tri*-PcNc/g-C_3N_4 system.

photoactivity for H_2 production originates from the excitation of Zn-*tri*-PcNc adsorbed on g-C_3N_4, and then the photogenerated electrons injected into the CB of g-C_3N_4 and further trapped by loaded co-catalyst Pt for H_2 production through water reduction. Simultaneously, the oxidized Zn-*tri*-PcNc will be regenerated by accepting electron from sacrificial reagent and then re-excited by light irradiation.

Since Zn-*tri*-PcNc shows a spectral response region of Zn-*tri*-PcNc centered at ~700 nm, and a marked increased photocurrent response of Zn-*tri*-PcNc/g-C_3N_4 can be observed after switching on 700 nm monochromatic light, as shown in Figure 6a, the photostability for H_2 production from Zn-*tri*-PcNc/g-C_3N_4 system was investigated under 700 nm monochromatic light irradiation. Based on the above-mentioned optimal condition, the photoreaction condition was slightly adjusted to 20 mg catalyst dispersed in 20 mL suspension containing AA in order to reduce the effect of water loss on photoactivity during the long-term irradiation and detection processes as far as possible. Moreover, a narrow band-pass 700 nm (BP700) filter is used to obtain $\lambda = 700 \pm 10$ nm monochromatic light irradiation; its transmission spectrum (Figure S5 in the Supporting Information) quite matches with the near-IR absorption of Zn-*tri*-PcNc, implying it can excite the adsorbed Zn-*tri*-PcNc but not the semiconductor.

Figure 9 depicts the long-term photostability for H_2 production of Zn-*tri*-PcNc/g-C_3N_4 system with/without adding CDCA under the above-mentioned conditions. As can be seen, Zn-*tri*-PcNc/g-C_3N_4 shows excellent photoactivity for H_2 production under 700 nm monochromatic light irradiation with rather good stability. Simultaneously, the coadsorption of CDCA can significantly enhance the photoactivity, especially giving an impressive average AOY value of 1.85% (in first 10 h) under 700 nm monochromatic light irradiation, which may be the highest AQY value at 700 nm monochromatic light, as far as we know. Although the photoactivity decreases to some extent during a second 10-h irradiation after remaining in darkness overnight, it still can be concluded that the present Zn-*tri*-PcNc/g-C_3N_4 leads to efficient utilization of near-IR light with extremely high AQY value.

Optical characterization was performed in an attempt to determine the reason for the aforementioned decrease in photoactivity. On the one hand, Zn-*tri*-PcNc/g-C_3N_4 after 10 h of light irradiation shows an absorption property and peak

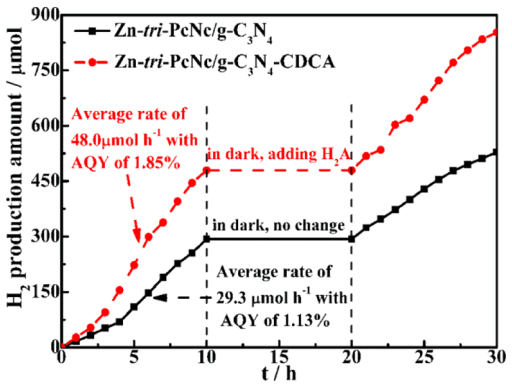

Figure 9. Long-term stability for H_2 production of Zn-*tri*-PcNc/g-C_3N_4 with/without adding coabsorbent CDCA under 700 nm monochromatic light irradiation.

position very similar to that without irradiation, as shown in Figure S5a in the Supporting Information, and there is no absorption signal of Zn-*tri*-PcNc in the filtrate of Zn-*tri*-PcNc/g-C_3N_4 suspension after 10 h of light irradiation, as shown in Figure S5b in the Supporting Information. The above results indicate that no Zn-*tri*-PcNc molecule desorbed from g-C_3N_4 and the spectral responsive ability did not change much after 10 h of irradiation. On the other hand, those desorbed samples with/without 10 h of irradiation, which are obtained by a desorption procedure (namely, catalyst was dispersed in 0.1 M NaOH in ethanol/water solution several times, and the liquid supernatant and precipitate were collected), also show DRS spectra very similar to the original one, as can be seen from Figure S5b in the Supporting Information. Moreover, the UV-vis absorption intensity of desorbed solutions of catalyst after 10 h of irradiation is just slightly less than that without irradiation. Therefore, it is reasonable to conjecture that there should be only a small proportion of Zn-*tri*-PcNc molecules lost through degradation or decomposition in the present aqueous suspension during the long-term stirring and irradiation, which should be responsible for the decrease of photoactivity for H_2 production to some extent. However, some other important factors, such as the accumulation of photogenerated species, along with the sacrificial reagent decomposition and the deactivation of catalyst under long-term residence in darkness, would also affect the photoactivity strongly, which requires further investigation.

4. CONCLUSION

Highly efficient dye-sensitized photocatalyst (Zn-*tri*-PcNc/g-C_3N_4) is constructed by combining asymmetric zinc phthalocyanine derivative (Zn-*tri*-PcNc) with intense near-infrared light (650−800 nm) absorption and polymeric graphitic carbon nitride (g-C_3N_4). It was found that Zn-*tri*-PcNc can extend the spectral response region of g-C_3N_4 from ~450 nm to more than 800 nm. After investigations on the photogenerated electron transfer process between Zn-*tri*-PcNc and g-C_3N_4 based on the thermodynamics and dynamics factors analyses, an optimal photoreaction condition was obtained for the Zn-*tri*-PcNc/g-C_3N_4 system. Especially, CDCA coadsorption with Zn-*tri*-PcNc can efficiently enhance the electron injection efficiency and retard the charge recombination, and thus resulting in significantly improved photoactivity for H_2 production. Under optimal photoreaction conditions, Zn-*tri*-PcNc/g-C_3N_4 with coadsorbent CDCA

dx.doi.org/10.1021/cs400863c | ACS Catal. 2014, 4, 162−170

exhibits high photoactivity (125.2 μmol h^{-1}) and turnover number (TON, ~5008 h^{-1}) for H_2 production under visible-light ($\lambda \geq 500$ nm) irradiation. Moreover, an extremely high apparent quantum yield (AQY, 1.85%) is obtained under 700 nm monochromatic light irradiation, which may be the highest AQY value observed at 700 nm monochromatic light irradiation, until now, as far as we know. The present work shows the promising application of phthalocyanine derivatives in photocatalytic H_2 production system for more efficiently utilizing the solar radiation with wavelength longer than 600 nm or even 700 nm, which has never been reached by the previous Ru-complexes and xanthenes dyes.

■ ASSOCIATED CONTENT

Supporting Information

XRD analysis, the investigation of photoreaction conditions, the effect of CDCA on DRS spectra of catalyst and the optical properties of the catalyst after irradiation are provided as Supporting Information. This material is available free of charge via the Internet at http://pubs.acs.org.

■ AUTHOR INFORMATION

Corresponding Author

*Tel./Fax: +86-27 6875 2237. E-mail: typeng@whu.edu.cn.

Notes

The authors declare no competing financial interest.

■ ACKNOWLEDGMENTS

This work was supported by the Natural Science Foundation of China (Nos. 21271146, 20871096, 21271144), the Program for New Century Excellent Talents in University of China (No. NCET-07-0637), and the Beijing National Laboratory for Molecular Sciences (BNLMS), China.

■ REFERENCES

(1) (a) Kubacka, A.; Fernández-García, M.; Colón, G. *Chem. Rev.* **2012**, *112*, 1555−1614. (b) Li, Y.; Fu, Z.; Su, B. *Adv. Funct. Mater.* **2012**, *22*, 4634−4667.
(2) (a) Nakata, K.; Fujishima, A. *J. Photochem. Photobiol. C* **2012**, *13*, 169−189. (b) Mlinar, V. *Nanotechnology* **2013**, *24*, 042001.
(3) (a) Chen, X.; Li, C.; Grätzel, M.; Kostecki, R.; Mao, S. S. *Chem. Soc. Rev.* **2012**, *41*, 7909−7937. (b) Dempsey, J.; Brunschwig, B.; Winkler, J.; Gray, H. *Acc. Chem. Res.* **2009**, *42*, 1995−2004.
(4) (a) Maeda, K. *J. Photochem. Photobiol. C* **2011**, *12*, 237−268. (b) Abe, R. *J. Photochem. Photobiol. C* **2010**, *11*, 179−209.
(5) (a) Qu, Y.; Duan, X. *Chem. Soc. Rev.* **2013**, *42*, 2568−2580. (b) Odobel, F.; Pellegrin, Y. *J. Phys. Chem. Lett.* **2013**, *4*, 2551−2564. (c) Teets, T.; Nocera, D. *Chem. Commun.* **2011**, *47*, 9268−9274.
(6) Zhang, X.; Veikko, U.; Mao, J.; Cai, P.; Peng, T. *Chem.—Eur. J.* **2012**, *18*, 12103−12111.
(7) Kudo, A.; Miseki, Y. *Chem. Soc. Rev.* **2009**, *38*, 253−278.
(8) (a) Li, K.; Chai, B.; Peng, T.; Mao, J.; Zan, L. *ACS Catal.* **2013**, *3*, 170−177. (b) Lakadamyali, F.; Reynal, A.; Kato, M.; Durrant, J. R.; Reisner, E. *Chem.—Eur. J.* **2012**, *18*, 15464−12457.
(9) (a) Peng, T.; Zhang, X.; Zeng, P.; Li, K.; Zhang, X.; Li, X. *J. Catal.* **2013**, *303*, 156−163. (b) Sun, Y.; Sun, J.; Long, J. R.; Yang, P.; Chang, C. J. *Chem. Sci.* **2013**, *4*, 118−124.
(10) Kim, W.; Tachikawa, T.; Majima, T.; Li, C.; Kim, H.; Choi, W. *Energy Environ. Sci.* **2010**, *3*, 1789−1795.
(11) (a) Kamegawa, T.; Matsuura, S.; Seto, H.; Yamashita, H. *Angew. Chem.* **2013**, *125*, 950−953. (b) Latorre-Sánchez, M.; Lavorato, C.; Puche, M.; Fornés, V.; Molinari, R.; Garcia, H. *Chem.—Eur. J.* **2012**, *18*, 16774−16783.
(12) Park, Y.; Kim, W.; Monllor-Satoca, D.; Tachikawa, T.; Majima, T.; Choi, W. *J. Phys. Chem. Lett.* **2013**, *4*, 189−194.
(13) Wang, X.; Maeda, K.; Thomas, A.; Takanabe, K.; Xin, G.; Carlsson, J. M.; Domen, K.; Antonietti, M. *Nat. Mater.* **2009**, *8*, 76−80.
(14) Wang, X.; Blechert, S.; Antonietti, M. *ACS Catal.* **2012**, *2*, 1596−1606.
(15) Wang, Y.; Wang, X.; Antonietti, M. *Angew. Chem., Int. Ed.* **2011**, *50*, 2−24.
(16) Liu, G.; Niu, P.; Sun, C.; Smith, S. C.; Chen, Z.; Lu, G.; Cheng, H. *J. Am. Chem. Soc.* **2010**, *132*, 11642−11648.
(17) Zhang, J.; Chen, X.; Takanabe, K.; Maeda, K.; Domen, K.; Epping, J.; Fu, X.; Antonietti, M.; Wang, X. *Angew. Chem., Int. Ed.* **2010**, *49*, 441−444.
(18) Chen, X.; Shen, S.; Guo, L.; Mao, S. S. *Chem. Rev.* **2010**, *110*, 6503−6570.
(19) Yan, H.; Huang, Y. *Chem. Commun.* **2011**, *47*, 4168−4170.
(20) Wang, Y.; Hong, J.; Zhang, W.; Xu, R. *Catal. Sci. Technol.* **2013**, *3*, 1703−1711.
(21) Min, S.; Lu, G. *J. Phys. Chem. C* **2012**, *116*, 1964419652.
(22) Takanabe, K.; Kamata, K.; Wang, X.; Antonietti, M.; Kubota, J.; Domen, K. *Phys. Chem. Chem. Phys.* **2010**, *12*, 13020−13025.
(23) (a) Yu, L.; Zhou, X.; Yin, Y.; Liu, Y.; Li, R.; Peng, T. *ChemPlusChem* **2012**, *77*, 1022−1027. (b) Ragoussi, M.; Cid, J.; Yum, J.; Torre, G.; Censo, D.; Grätzel, M.; Nazeeruddin, M.; Torres, T. *Angew. Chem., Int. Ed.* **2012**, *51*, 4375−4378. (c) García-Iglesias, M.; Yum, J.; Humphry-Baker, R.; Zakeeruddin, S.; Péchy, P.; Vázquez, P.; Palomares, E.; Grätzel, M.; Nazeeruddin, M.; Torres, T. *Chem. Sci.* **2011**, *2*, 1145−1150.
(24) Zhang, X.; Yu, L.; Zhuang, C.; Peng, T.; Li, R.; Li, X. *RSC Adv.* **2013**, *3*, 14363−14370.
(25) Tum, J.; Jang, S.; Humphry-Baker, R.; Grätzel, M.; Cid, J.; Torres, T.; Nazeeruddin, M. *Langmuir* **2008**, *24*, 5636−5640.
(26) Mao, J.; Peng, T.; Zhang, X.; Li, K.; Ye, L.; Zan, L. *Catal. Sci. Technol.* **2013**, *3*, 1253−1260.
(27) Kim, Y.; Park, H. *Energy Environ. Sci.* **2011**, *4*, 685−694.
(28) Abe, R.; Hara, K.; Sayama, K.; Domen, K.; Arakawa, H. *J. Photochem. Photobiol. A* **2000**, *137*, 63−69.
(29) (a) Xu, J.; Li, Y.; Peng, S.; Lu, G.; Li, S. *Phys. Chem. Chem. Phys.* **2013**, *15*, 7657−7665. (b) Chai, B.; Peng, T.; Mao, J.; Li, K.; Zan, L. *Phys. Chem. Chem. Phys.* **2012**, *14*, 16745−16752.
(30) Liu, Y.; Liu, C.; Liu, Y. *Appl. Surf. Sci.* **2011**, *257*, 5513−5518.
(31) Jin, Z.; Zhang, X.; Li, Y.; Li, S.; Lu, G. *Catal. Commun.* **2007**, *8*, 1267−1273.
(32) Choi, S.; Yang, H.; Kim, J.; Park, H. *Appl. Catal., B* **2012**, *121*−*122*, 206−213.
(33) (a) Abe, R.; Hara, K.; Sayama, K.; Domen, K.; Arakawa, H. *J. Photochem. Photobiol. A* **2000**, *137*, 63−69. (b) Sun, H.; Hoffman, M. *J. Phys. Chem.* **1994**, *98*, 11719−11726.
(34) Han, Z.; Qiu, F.; Eisenberg, R.; Holland, P.; Krauss, T. *Science* **2012**, *338*, 1321−1324.
(35) Bae, E.; Choi, W. *J. Phys. Chem. B* **2006**, *110*, 14792−14799.